Optics Letters

Resolving adjacent 20-cm hot spots over 2.5 km in Raman distributed optical fiber sensing via optimal chaotic segment correlation

Ziheng Yan,[1,2] Zhiwei Lin,[1,2] Xizhen Xu,[1,2] Yiping Wang,[1,2] and Jun He[1,2,*]

[1]State Key Laboratory of Radio Frequency Heterogeneous Integration, Key Laboratory of Optoelectronic Devices and Systems of Ministry of Education/Guangdong Province, College of Physics and Optoelectronic Engineering, Shenzhen University, Shenzhen 518060, China
[2]Shenzhen Key Laboratory of Photonic Devices and Sensing Systems for Internet of Things, Guangdong and Hong Kong Joint Research Centre for Optical Fiber Sensors, Shenzhen University, Shenzhen 518060, China
*hejun07@szu.edu.cn

Received 22 July 2026; revised 21 August 2026; accepted 4 September 2026; posted 8 September 2026; published 25 September 2026

Resolving adjacent submeter-scale hot spots in Raman distributed temperature sensing (DTS) is critically limited by the finite pump-pulse duration. This pulse-width-limited spatial resolution inherently merges thermal responses from nearby events into an overlapped profile. Chaotic Raman DTS can overcome the pulse-width limitation in principle. However, the correlation peaks still broaden and overlap when multiple hot spots are adjacent, preventing reliable identification of individual events. Here, we propose and demonstrate an optimal chaotic segment correlation (OCSC) method that exploits the nonuniform local correlation property of a broadband chaotic pulse. A 1-ns sliding window is applied to a 50-ns chaotic reference pulse to select the segment with the minimum autocorrelation full width at half maximum (FWHM), and this optimal segment is then used as the correlation kernel against a self-differentially reconstructed Raman anti-Stokes signal. This local-reference strategy effectively suppresses redundant correlation components arising from the full pulse and enhances the separability of adjacent temperature-induced responses. In the experiment, two adjacent 20-cm hot spots with 60-cm separation are clearly resolved at a distance of 2.52 km, with consistent demodulation performance obtained at 60, 70, and 80°C. The proposed OCSC method provides a general signal-processing route for multi-event discrimination in correlation-based distributed fiber sensors that use chaotic laser or random light sources. © 2026 Optica Publishing Group. All rights, including for text and data mining (TDM), Artificial Intelligence (AI) training, and similar technologies, are reserved.

https://doi.org/10.1364/OL.611972

Distributed temperature sensing (DTS) based on Raman optical time-domain reflectometry (OTDR) is one of the most mature sensing techniques for long-range thermal monitoring, owing to its simple configuration, immunity to electromagnetic interference, and intrinsic temperature sensitivity [1–3]. It has been widely deployed in power cables, fire detection, oil and gas pipelines, tunnels, and energy infrastructure [4,5]. In these applications, incipient thermal anomalies typically manifest as localized submeter-scale hot spots rather than extended meter-scale heated zones [6,7]. Multiple such hot spots may occur within a short fiber span, making their individual responses difficult to distinguish. Accurate identification of their positions, lengths, separations, and temperatures is essential for early warning [8,9].

In conventional Raman-OTDR, spatial resolution is intrinsically limited by the pump-pulse width and time-of-flight principle [10]. Various methods have been developed to overcome this limitation. For example, DTS with 10-cm spatial resolution over 500 m was achieved using a superconducting nanowire-based single-photon detector [11], while DTS with 0.25-m resolution was achieved using a reconstruction algorithm [12]. In 2024, Dong *et al.* achieved a 1-cm resolution using a fiber solenoid [13]. Pulse-width compression and solenoid-based schemes can improve spatial resolution but generally restrict the sensing range, making it difficult to maintain kilometer-scale performance.

To extend the sensing distance while preserving high spatial resolution, various solutions have been explored, including few-mode fiber sensing [14], pulse-coded modulation [15], and chaotic laser correlation demodulation [16,17]. For example, in 2017, Tang *et al.* utilized few-mode fibers to achieve 3.0-m resolution over 20.0 km [14]. In 2020, Sun *et al.* demonstrated DTS with 1-m resolution over 39.0 km via a single-sequence aperiodic code [18]. In the field of chaos correlation Raman DTS, Wang *et al.* established a second-order correlation demodulation framework and achieved 10-cm resolution over 1.4 km [19]. Subsequently, Fan *et al.* proposed a chaotic asymmetric paired-pulse correlation-enhanced scheme, achieving 30-cm resolution over 10 km [20], and 30-cm resolution over 6.0 km was recently demonstrated using chaotic pulse cluster demodulation [21]. These studies have exhibited the capability of chaotic Raman sensing to localize a single submeter-scale hot spot [22]. However, the Raman responses from different hot spots remain coupled within the finite pulse-width response, producing overlapping features in the measured temperature trace.

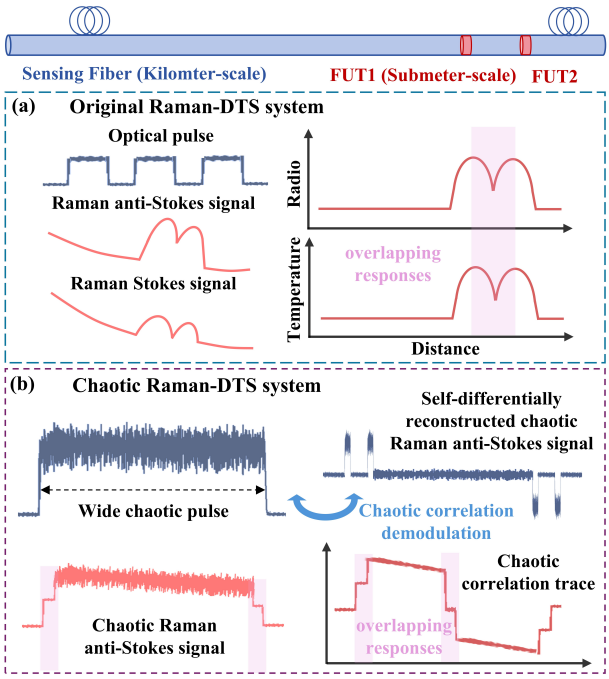


Fig. 1. Superposition of Raman backscattered signals from multiple closely spaced submeter-scale hot spots. (a) Conventional Raman DTS. (b) Chaotic Raman DTS.

Consequently, the quantitative discrimination of multiple adjacent submeter-scale hot spots remains inadequately addressed.

In this Letter, we propose and demonstrate an optimal chaotic segment correlation (OCSC) method for discriminating multiple adjacent submeter-scale hot spots in chaotic Raman DTS. Instead of using the entire broad chaotic pulse as the correlation reference, we apply a fixed-length sliding window to search for a 1-ns segment with the minimum autocorrelation FWHM. The 1-ns segment is selected as the shortest effective correlation reference for resolving multiple closely spaced hot spots under the current experimental conditions. This optimal segment is then correlated with a self-differentially reconstructed Raman anti-Stokes signal. Numerical simulation results can verify the discrimination of multiple submeter-scale hot spots. In experiments, two 20-cm hot spots separated by 60 cm are clearly resolved at 2.52 km, with consistent results at 60, 70, and 80 °C. This approach provides a new pathway for adjacent hot-spot discrimination in chaotic Raman DTS systems.

In conventional Raman DTS, when the lengths and separations of adjacent hot spots are shorter than the pump-pulse width, the anti-Stokes and Stokes responses broaden and overlap. The resulting temperature trace fails to resolve the individual hot spots, as illustrated in Fig. 1(a). Chaotic Raman DTS replaces pulse time-of-flight localization with correlation-based demodulation [16]. In this scheme, the entire broad chaotic pulse serves as the reference. After differential reconstruction of the Raman anti-Stokes signal, temperature is recovered at the boundaries of the heated regions, as shown in Fig. 1(b). However, using the full chaotic pulse as the reference introduces redundant low-correlation components. Consequently, multiple closely spaced hot spots produce overlapping bipolar correlation features, leading to unreliable localization and temperature demodulation.

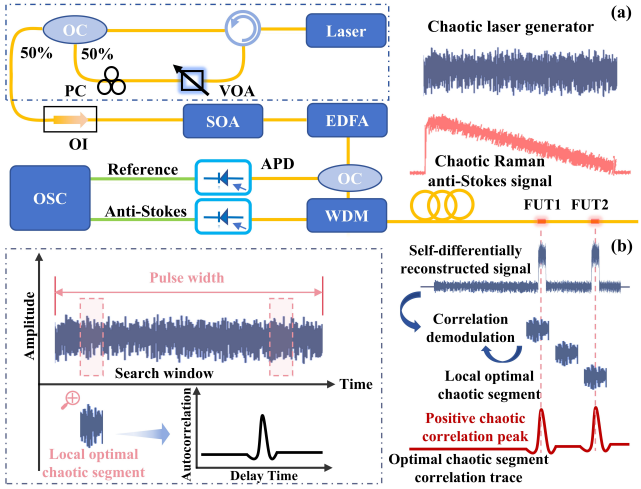


Fig. 2. Hardware architecture and signal processing flowchart of the chaotic Raman DTS. (a) Schematic diagram of the experimental setup. (b) Signal processing procedure of the OCSC method for discriminating multiple adjacent hot spots.

The experimental setup of chaotic Raman DTS is shown in Fig. 2(a). A 1550-nm continuous-wave laser passes through an optical circulator and is modulated into continuous chaotic light via a single-feedback loop [17], comprising a variable optical attenuator (VOA), a polarization controller (PC), and a 50:50 fiber coupler (OC). This continuous chaotic laser is then modulated into a pulsed chaotic laser via an optical isolator (OI) and a semiconductor optical amplifier (SOA) and subsequently amplified by an erbium-doped fiber amplifier (EDFA). The chaotic pulse is split into two paths by an OC: one serves as the reference signal for correlation processing, and the other is launched into the sensing fiber through a wavelength-division multiplexer (WDM). Both the anti-Stokes signal and the reference pulse are detected by two avalanche photodiodes (APDs, 400 MHz bandwidth) and recorded by an oscilloscope (OSC). The OCSC window length is coupled to the detection bandwidth; as the bandwidth decreases, the minimum identifiable hot spot length increases. Moderate down-sampling is feasible, provided the band-limited chaotic waveform remains sufficiently sampled for autocorrelation-FWHM estimation and correlation positioning. The fiber under test (FUT) is a 50/125 graded-index multimode fiber (MMF).

The signal-processing procedure for the OCSC-assisted chaotic Raman DTS is illustrated in Fig. 2(b). Different from a predetermined or arbitrarily truncated local correlation reference, OCSC adaptively selects the correlation segment based on the autocorrelation characteristics of the synchronously acquired chaotic pulse. First, the measured Raman anti-Stokes trace is processed by adjacent-point self-differencing to recover the chaotic fluctuations induced by temperature changes. Then, a nanosecond-scale sliding window is applied to the chaotic reference pulse to search for the optimal segment exhibiting the sharpest autocorrelation peak (i.e., minimum FWHM). This selected segment is then correlated with the reconstructed signal. Finally, adjacent submeter-scale hot spots are resolved by identifying the positions of the positive correlation peaks.

As shown in Fig. 3, numerical simulation was carried out to study the performance of the OCSC method. Two temperature configurations were studied: two 20-cm hot spots separated

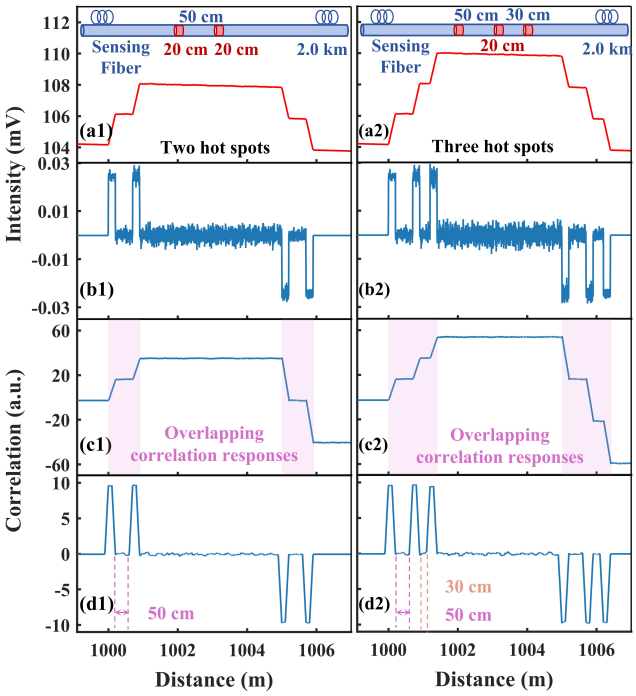


Fig. 3. Simulation results for resolving multiple submeter-scale hot spots. (a1) and (a2) Raman anti-Stokes traces for two and three 20-cm hot spots; (b1) and (b2) corresponding self-differentially reconstructed signals; (c1) and (c2) conventional full-pulse chaotic correlation results; and (d1) and (d2) OCSC demodulation results.

by 50 cm; and three 20-cm hot spots with separations of 50 and 30 cm. The simulated Raman anti-Stokes traces are presented in Figs. 3(a1) and 3(a2). Figures 3(b1) and 3(b2) show the corresponding self-differentially reconstructed signals, in which chaotic fluctuation features are recovered at the rising and falling boundaries of each hot spot. However, conventional full-pulse chaotic correlation produces broadened and overlapping responses for multiple hot spots, as shown in Figs. 3(c1) and 3(c2) [19]. In contrast, the OCSC results in Figs. 3(d1) and 3(d2) demonstrate distinct positive correlation peaks associated with the different hot spots, successfully resolving two hot spots separated by 50 cm and three hot spots with separations of 50 and 30 cm.

The optimal chaotic segment was selected from a 50-ns reference pulse using a 1-ns sliding window. As shown in Fig. 4(a), the autocorrelation FWHM varies substantially with the temporal position of the window; the segment corresponding to the minimum FWHM is marked by the red star. Figure 4(b) highlights the selected 1-ns segment within the measured 50-ns chaotic pulse time series. Its normalized autocorrelation function, shown in Fig. 4(c), exhibits a pronounced central peak and relatively low off-peak fluctuations. These results confirm that the local correlation performance of a broad chaotic pulse is nonuniform, providing a basis for selecting an effective correlation template.

Subsequently, the experimental performance of the OCSC method was evaluated using two 20-cm hot spots separated by 60 cm near the end of a 2.52-km sensing fiber. Figure 5(a) shows the measured Raman anti-Stokes trace at 80 °C, with the inset plot zooming in on the region from 2418 to 2430 m. The two hot spots manifest as a single broadened response in the

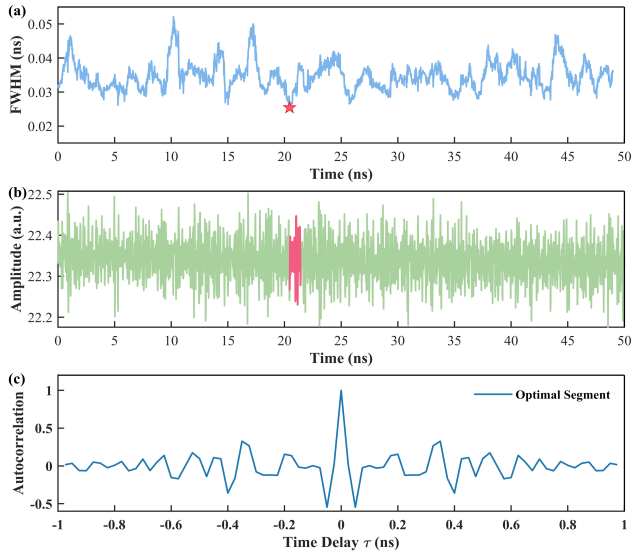


Fig. 4. Selection and autocorrelation characterization of the optimal chaotic segment. (a) FWHM as a function of the temporal position of a 1-ns sliding window applied to the 50-ns chaotic pulse; the minimum is marked by the red star. (b) Measured 50-ns chaotic pulse time series with the selected 1-ns segment highlighted in red. (c) Normalized autocorrelation of the optimal segment.

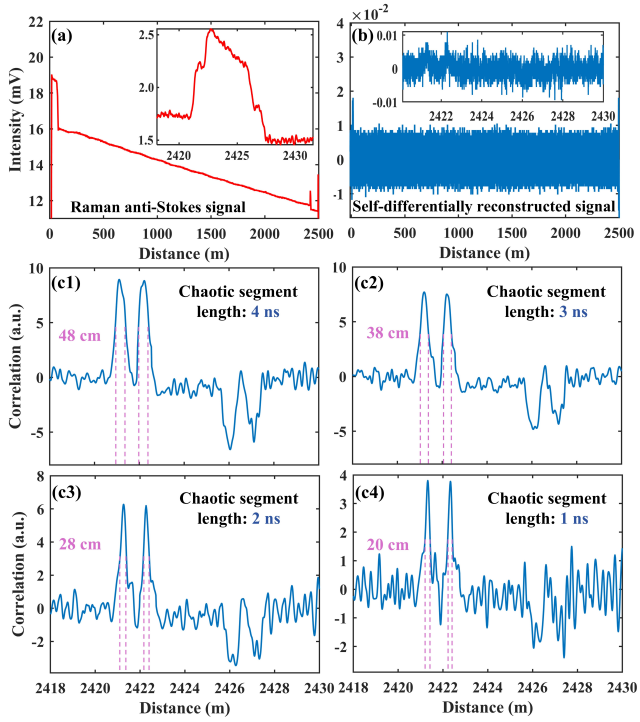


Fig. 5. Experimental results for two 20-cm hot spots separated by 60 cm. (a) Measured Raman anti-Stokes trace; (b) self-differentially reconstructed signal; and (c1)–(c4) OCSC demodulation results obtained using chaotic segment lengths of 4, 3, 2, and 1 ns, respectively.

raw trace and cannot be directly resolved. The reconstructed signal, presented in Fig. 5(b), exhibits weak chaotic fluctuation features associated with the hot-spot boundaries, although these features remain partially obscured by background noise.

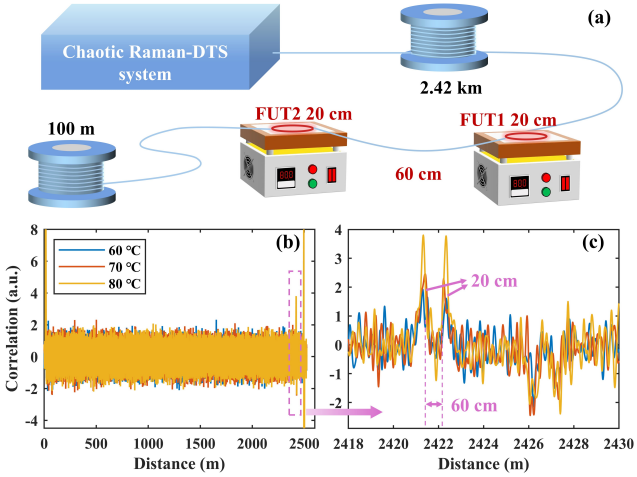


Fig. 6. Experimental discrimination of two adjacent submeter-scale hot spots. (a) Experimental arrangement with two 20-cm hot spots separated by 60 cm; (b) OCSC demodulation traces over the entire sensing fiber at 60, 70, and 80°C; and (c) enlarged view of the region from 2418 to 2430 m.

Figures 5(c1)–5(c4) show the OCSC results obtained using chaotic segment lengths of 4, 3, 2, and 1 ns, respectively. Reducing the segment from 4 to 1 ns narrows the correlation-response width (48 to 20 cm) at the cost of the signal-to-noise ratio (a decrease of 6.3 dB). Considering the 0.88 ns response time of the 400-MHz APD, the 1-ns length was selected as the shortest effective window.

Moreover, the discrimination capability for adjacent submeter-scale hot spots was further evaluated at different temperatures. The experimental arrangement is shown in Fig. 6(a). Two 20-cm fiber sections were independently heated with a 60-cm separation at 2.42 km. Figure 6(b) illustrates the OCSC demodulation traces over the entire sensing fiber at 60, 70, and 80°C. The hot spots are localized near the fiber end, with no comparable correlation features observed elsewhere along the fiber. Figure 6(c) shows the enlarged demodulation results from 2418 to 2430 m. Two positive correlation peaks are observed at all three temperatures, and their positions remain consistent with the preset hot-spot locations. The peak amplitudes increase with temperature because of the enhanced Raman anti-Stokes response, while the measured spatial positions and separation remain stable. The noise robustness of 1-ns OCSC was further evaluated by adding Gaussian noise to the measured Raman signal at 80°C. The minimum correlation SNR of the four boundary responses decreased from 15.80 to 6.95 dB, while the adjacent hot spots remained distinguishable with stable boundary positions.

In summary, we have demonstrated an OCSC-assisted chaotic Raman DTS technology that exploits the nonuniform local correlation property within a broad chaotic pulse. By selecting a 1-ns segment with the narrowest autocorrelation FWHM and correlating it with the self-differentially reconstructed Raman anti-Stokes signal, overlapping full-pulse correlation responses are converted into distinguishable features. The method resolves multiple adjacent submeter-scale hot spots in simulation and experimentally distinguishes two 20-cm hot spots with a 60-cm separation at 2.52 km under temperatures of 60, 70, and 80°C. The proposed approach offers a promising signal-processing pathway for multi-event discrimination in correlation-based distributed fiber sensors, with potential applications in harsh environments such as aerospace vehicles, nuclear plants, and oil and gas exploration.

Funding. National Natural Science Foundation of China (62435012, U25B2051); Department of Science and Technology of Guangdong Province (2026A1515011451, 2024TQ08Z673); Shenzhen Key Laboratory of Photonic Devices and Sensing Systems for Internet of Things (SYSPG20241211173908021); Scientific Foundation for Youth Scholars of Shenzhen University (868-000001033425).

Disclosures. The authors declare no conflicts of interest.

Data availability. Data underlying the results presented in this paper are not publicly available at this time but may be obtained from the authors upon reasonable request.

REFERENCES

1. W. Zhan, M. Cantono, V. Kamalov, *et al.*, Science **371**, 931 (2021).
2. Z. Yan, B. Du, J. He, *et al.*, J. Lightwave Technol. **43**, 9465 (2025).
3. Z. Li, Q. Tan, Z. Yan, *et al.*, Optics Laser Technol. **182**, 112185 (2025).
4. G. Liu, H. Meng, G. Qu, *et al.*, J. Build. Eng. **70**, 106403 (2023).
5. L. C. B. Silva, M. E. V. Segatto, and C. E. S. Castellani, Opt. Fiber Technol. **74**, 103091 (2022).
6. A. R. Bahrampour and F. Maasoumi, Opt. Fiber Technol. **16**, 240 (2010).
7. T. Dong, Z. Ma, X. Liu, *et al.*, Measurement **267**, 120563 (2026).
8. Y. Zhu, X. Fan, Y. Wan, *et al.*, Chin. Opt. Lett. **23**, 091201 (2025).
9. Z. Pan, M. Peng, Y. Gao, *et al.*, Chin. Opt. Lett. **23**, 111202 (2025).
10. B. Liu, M. P. Buric, B. T. Chorpening, *et al.*, J. Lightwave Technol. **36**, 5511 (2018).
11. J. Gasser, D. Warpelin, F. Bussières, *et al.*, Opt. Express **30**, 6768 (2022).
12. Z. Xu, J. Ling, W. Ye, *et al.*, IEEE Sensors J. **23**, 10500 (2023).
13. P. Chen, T. Zhang, and X. Dong, Measurement **230**, 114538 (2024).
14. M. Wang, H. Wu, M. Tang, *et al.*, Opt. Express **25**, 4907 (2017).
15. Y. Zhou, L. Yan, Z. Li, *et al.*, Opt. Lett. **48**, 3143 (2023).
16. R. Zhou, F. Chen, S. Li, *et al.*, J. Lightwave Technol. **39**, 3244 (2021).
17. J. Li, C. Wang, K. Cao, *et al.*, APL Photonics **8**, 076105 (2023).
18. X. Sun, Z. Yang, X. Hong, *et al.*, Nat. Commun. **11**, 5774 (2020).
19. C. Wang, J. Li, X. Zhou, *et al.*, Light Sci. Appl. **12**, 213 (2023).
20. B. Fan, J. Li, Z. Cheng, *et al.*, Photon. Res. **12**, 2365 (2024).
21. J. Li, Z. Cheng, B. Fan, *et al.*, Adv. Photon. Nexus **4**, 046011 (2025).
22. Y. Sun, Y. Luo, H. Liu, *et al.*, PhotoniX **6**, 31 (2025).